Journal of Applied Polymer Science

Comparison of the Effects of Phenyl Dichlorophosphate Modified and Unmodified β-Iron(III) Oxide Hydroxide on the Thermal, Combustion, and Mechanical Properties of Ethylene–Vinyl Acetate/Magnesium Hydroxide Composites

Lei Wang,[1,3] Jing Zhan,[1] Lei Song,[1] Yuan Hu,[1,3] Richard K. K. Yuen[2]

[1]State Key Laboratory of Fire Science, University of Science and Technology of China, 96 Jinzhai Road, Hefei, Anhui 230026, People's Republic of China

[2]Department of Civil and Architectural Engineering, City University of Hong Kong and University of Science and Technology of China-City University of Hong Kong Joint Advanced Research Centre, Hong Kong, People's Republic of China

[3]Suzhou Key Laboratory of Urban Public Safety, Suzhou Institute of University of Science and Technology of China, Suzhou, People's Republic of China

Correspondence to: Y. Hu (E-mail: yuanhu@ustc.edu.cn) or L. Song (E-mail: leisong@ustc.edu.cn)

ABSTRACT: The objective of this study was to compare the impact of β-iron(III) oxide hydroxide [β-Fe(O)OH] and iron hydroxide modified with phenyl dichlorophosphate [β-Fe(O)OPDCP] on the thermal, combustion, and mechanical properties of ethylene–vinyl acetate (EVA)/magnesium hydroxide (MH) composites. For the EVA/MH composites in combination with these iron-containing co-additives, β-Fe(O)OH and β-Fe(O)OPDCP both led to an increase in the thermal stability at higher temperatures. The results of microscale combustion calorimetry indicate that the peak heat-release rate, total heat release, and heat-release capacity, which are indicators of a material fire hazard, all decreased. Moreover, significant improvements were obtained in the limiting oxygen index (LOI) and Underwriters Laboratories 94 ratings. However, the EVA4 system reached a V-0 rating, whereas the EVA3 system reached a V-2 rating. The LOI values for the EVA3 and EVA4 systems were 35 and 39, respectively. A homogeneous and solid structure of char residue caused by β-Fe(O)OPDCP was observed by scanning electron microscopy. Furthermore, because of the good interfacial compatibility between the fillers and the EVA matrix, the EVA4 system presented better mechanical properties than the EVA3 system. Thermogravimetric analysis/IR spectrometry showed that β-Fe(O)OPDCP reduced the combustible volatilized products of EVA/MH.
 J. Appl. Polym. Sci. **2014**, *131*, 40112.

KEYWORDS: composites; mechanical properties; thermogravimetric analysis (TGA)

Received 27 June 2013; accepted 21 October 2013

DOI: 10.1002/app.40112

INTRODUCTION

Ethylene–vinyl acetate (EVA) copolymers with different vinyl acetate (VA) contents are used extensively in many fields, especially in the cable industry, as excellent insulating materials with good physical and chemical properties.[1] However, their development and application are greatly limited by their high flammability. In past decades, halogenated compounds were commonly used as fillers to improve the fire retardancy of EVA.[2] Unfortunately, their fire-retardant action is accompanied by negative effects, such as the generation of corrosive, obscuring, toxic smoke. In addition, the manufacture and application of some halogen-containing flame retardants are restricted by new regulations. It is well known that fire retardancy can be achieved with hydrated mineral fillers, such as alumina trihydrate or magnesium hydroxide (MH),[3,4] which are excellent nontoxic, smoke-suppressing, halogen-free flame-retardant additives. These compounds act in both the condensed and gas phases and decompose according to an endothermic reaction; this reduces the temperature of materials and releases water to the gaseous phases. However, high filler contents are often required to obtain satisfactory fire-related properties. A small amount of co-additives often bring significant improvements to their thermal stability and flame-retardant properties; this implies that these co-additives can enhance their efficiencies. Many compounds have been used as co-additives; these include fumed silica, zeolite, lanthanum

Table I. TGA Results for the EVA, EVA/MH, and EVA/MH/Iron Compound Formulations

Sample	Composition	T_{-10}	T_{-50}	Residue at 700°C (%)
EVA1	EVA	365 ± 1	468 ± 1	0.1 ± 0.2
EVA2	EVA/55% MH	361 ± 1	484 ± 1	35.2 ± 0.2
EVA3	EVA/54% MH/1% β-Fe(O)OH	356 ± 1	485 ± 1	38.6 ± 0.2
EVA4	EVA/54% MH/1% β-Fe(O)OPDCP	360 ± 1	488 ± 1	38.8 ± 0.2

oxide, iron compounds, and α-zirconium phosphate.[5–9] The efficiency of some iron compounds that have been reported to be used as co-additives is obvious.[5,6] The effect of the incorporation of a butyl acrylate–iron chelate resin on the flammability properties of MH–low-density polyethylene compositions was investigated. It was found that the resin–iron chelate had a remarkable effect on the flammability properties of low-density polyethylene compositions.[5] The influence of iron montmorillonite (Fe-MMT) on the fire retarding behavior and mechanical properties of an EVA copolymer/MH composite was studied. The results demonstrate that compared with that of sodium montmorillonite, the synergistic effects of Fe-MMT enhanced the limiting oxygen index (LOI) value of the EVA/MH composite, improved the thermal stability, and reduced the heat release rate (HRR). The 45% EVA/53% MH/2% Fe-MMT composite passed the V-0 test.[6] However, modified or unmodified β-iron(III) oxide hydroxide [β-Fe(O)OH] as a co-additive in polymer/flame-retardant composites has not yet been studied.

In this study, iron hydroxide modified with phenyl dichlorophosphate [β-Fe(O)OPDCP] was prepared and used as a co-additive to improve the flame retardancy of an EVA/MH composite. To understand the impact of β-Fe(O)OPDCP on the flaming and mechanical properties of the EVA/MH composite, the effect of β-Fe(O)OH on the properties of the EVA/MH composite was also studied. Comparative tests of the thermal performance, flammability, and mechanical properties of the composite materials were conducted by thermogravimetric analysis (TGA), LOI testing, Underwriters Laboratories 94 (UL 94) ratings, microscale combustion calorimetry (MCC), a universal testing machine, and dynamic mechanical thermal analysis (DMTA). Some inference in the mode of action of the flame retardants was observed in the scanning electron microscopy (SEM) images of their residue chars. The volatilized products after the thermal decomposition of samples were analyzed by TGA–IR spectrometry.

EXPERIMENTAL

Materials

Phenyl dichlorophosphate (PDCP), iron(III) chloride hexahydrate ($FeCl_3 \cdot 6H_2O$), and tetrahydrofuran were purchased from Sinopharm Chemical Reagent Co., Ltd. These reagents were of analytical grade and were used without further purification. MH was kindly provided by KeYan Co. (Hefei, China). The EVA copolymer, containing 28 wt % VA, was supplied by Hanwha CO., Ltd. (Korea).

Preparation of β-Fe(O)OPDCP

β-Fe(O)OH was prepared by a typical experiment,[10,11] FeCl3 (0.487 g) was dissolved in distilled water (30 mL) under stirring. Then, the mixture was transferred to a 40-mL Teflon-lined autoclave. Hydrothermal synthesis was carried out in an oven at 110°C for 2 h. The products were collected by filtration, washed with distilled water and ethanol several times, and then dried in an oven at 60°C for 6 h.

Surface modification of β-Fe(O)OH was prepared by the mixture of 10 mL of PDCP with 1 g of β-Fe(O)OH. After it was shaken for a short time, the mixture was moved into a three-necked, round-bottom flask. Then, water (20 mL) was slowly added in to the three-necked, round-bottom flask at 10°C for 5 h. Thereafter, the product was filtered and washed with low-density polyethylene on a Soxhlet extractor for over 36 h. Finally, the particles were dried at 60°C in an oven for 24 h. The obtained particles were labeled β-Fe(O)OPDCP.

Preparation of the Samples

EVA, MH, β-Fe(O)OH, and β-Fe(O)OPDCP were dried in an oven at 80°C overnight before use. They were melt-mixed in a twin-roller mill (KX-160, Jiangsu, China) for 10 min at the same time. The temperature of the mill was maintained at 130°C, and the roller speed was 100 rpm for the preparation of all of the samples listed in Table I. The resulting systems were hot-pressed into sheets of suitable thickness and size for LOI and UL 94 tests. Dumbbell-shaped specimens for the universal testing machine were prepared according to ASTM D 412.

Characterization

X-Ray Diffraction (XRD) Analysis. XRD patterns were obtained on 1 mm thick films with a Japan Rigaku D/Max-Ra rotating anode X-ray diffractometer equipped with a Cu Kα tube and Ni filter (11/40.1542 nm).

SEM. The SEM image of the residue after the LOI tests was taken with a DXS-10 scanning electron microscope produced by Shanghai Electron Optical Technology Institute. The char was observed on the copper plate and then coated with a gold/palladium alloy to prepare it for imaging.

Fourier Transform Infrared (FTIR) Spectroscopy. FTIR spectroscopy (Nicolet 6700 FTIR spectrophotometer, Thermo Fisher Scientific) was used to characterize the samples with thin KBr discs. The transmission mode was used, and the wave-number range was set from 4000 to 400 cm^{-1}.

X-Ray Photoelectron Spectroscopy (XPS). XPS measurement was carried out with a VG ESCALB MK-II electron spectrometer. The excitation source was an AlKα line at

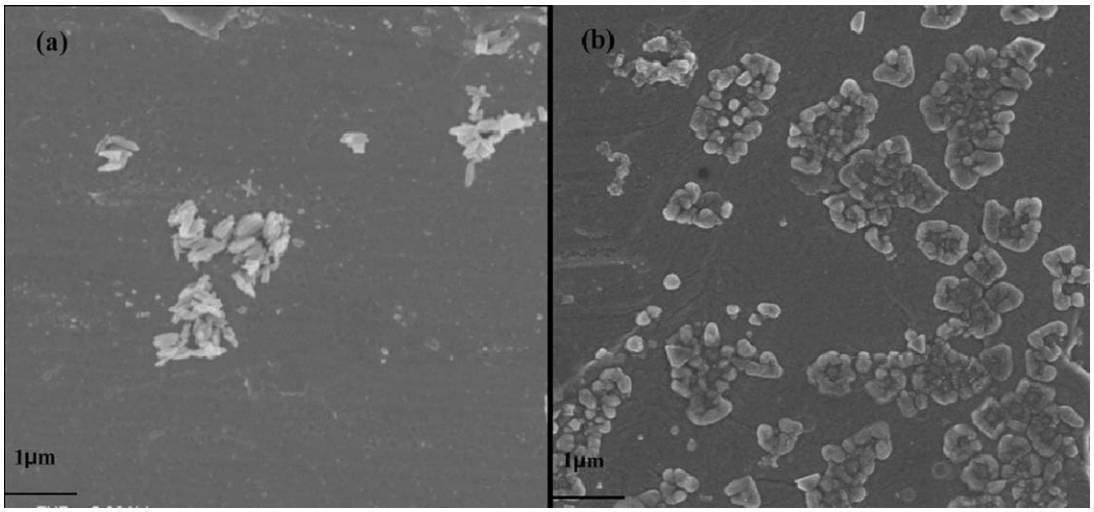

Figure 1. SEM of (a) β-Fe(O)OH and (b) β-Fe(O)OPDCP.

1486.6 eV. Elemental analysis was carried out with an inductively coupled plasma mass spectrometer (Plasma Quad 3).

TGA. Each sample was examined in a nitrogen atmosphere flowing at 150 mL/min on a Q5000 thermogravimetric analyzer (TA Instruments) at a heating rate of 20°C/min. The weight of all of the samples was kept within 3–10 mg in an open Pt pan and heated from room temperature to 700°C. The temperature reproducibility of the instrument was ±1°C, whereas the mass reproducibility was ±0.2%.

LOI. LOI was measured with an HC-2 oxygen index meter (Jiang Ning Analysis Instrument Co., China) on 100 × 6.7 × 3 mm^3 sheets according to the standard oxygen index test ASTM D 2863-77.

UL 94 Vertical Burning Test. The vertical burning test was conducted with a CZF-II horizontal and vertical burning tester (Jiang Ning Analysis Instrument Co., China). The specimens used were 127 × 12.7 × 3 mm^3 according to the UL 94 test ASTM D 3801-1996 standard.

MCC. Microscale combustion calorimetry (MCC, Govmark) was used to analyze the combustion properties of the samples according to ASTM D 7309-7. For each sample 4 – 6 mg was heated to 600 at 1°C/s in a stream of nitrogen flowing at 80cm^3/min. The volatile anaerobic thermal degradation products in the nitrogen gas stream were mixed with a 20cm^3/min stream of pure oxygen prior to entering a 900°C combustion furnace. The MCC data obtained were reproducible to about 3%.

Mechanical Properties. The mechanical properties were measured with a universal testing machine (Instron model 1185) at temperatures of 25 ± 2°C according to ASTM D 412. The crosshead speed was 200 mm/min. The tensile strength (TS) and elongation at break (E_b) were also recorded.

DMTA. DMTA was performed on a PerkinElmer Diamond DMA (MA) at a constant frequency of 10 Hz and a heating rate of 5°C/min over the range of −50 to 50°C.

TGA–IR Spectrometry. TGA–IR spectrometry was performed to analyze the volatilized products after the pyrolysis of the samples under a nitrogen flow of 20.0 mL/min.

RESULTS AND DISCUSSION

Characterization of the Modifiers

Figure 1(a) displays the SEM image of the sample, in which spindle-shaped particles were produced with an average width of 50 nm and length of 300 nm (aspect ratio ≈ 1:6). Compared with that in Figure 1(b), the shape of the modified products changed significantly from a spindle to a small rod with a smooth surface after the introduction of PDCP. The XRD pattern (Figure 2) of β-Fe(O)OH was in agreement with that previously reported in the literature.[12]

XPS analysis was carried out to determine the surface composition of β-Fe(O)OH and β-Fe(O)OPDCP. The X-ray photoelectron spectra of the samples are shown in Figure 3. The peaks turning up in the spectra included the C1s, O1s, Fe2p, and P2p peaks. As shown in Figure 3, the iron elemental content of the sample surface was significantly reduced, and the electron binding energy peak of the phosphorus element appeared after

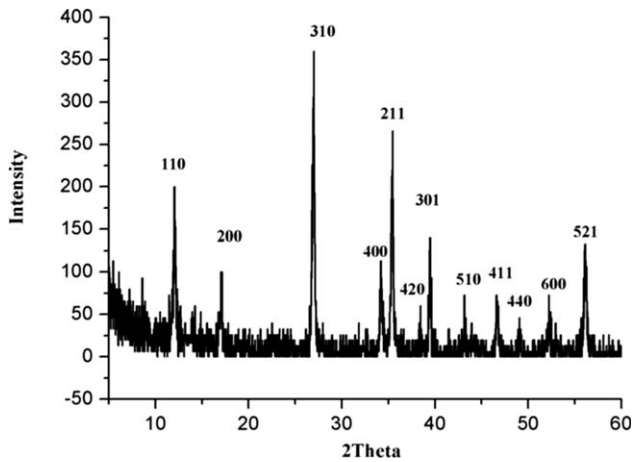

Figure 2. XRD pattern of β-Fe(O)OH.

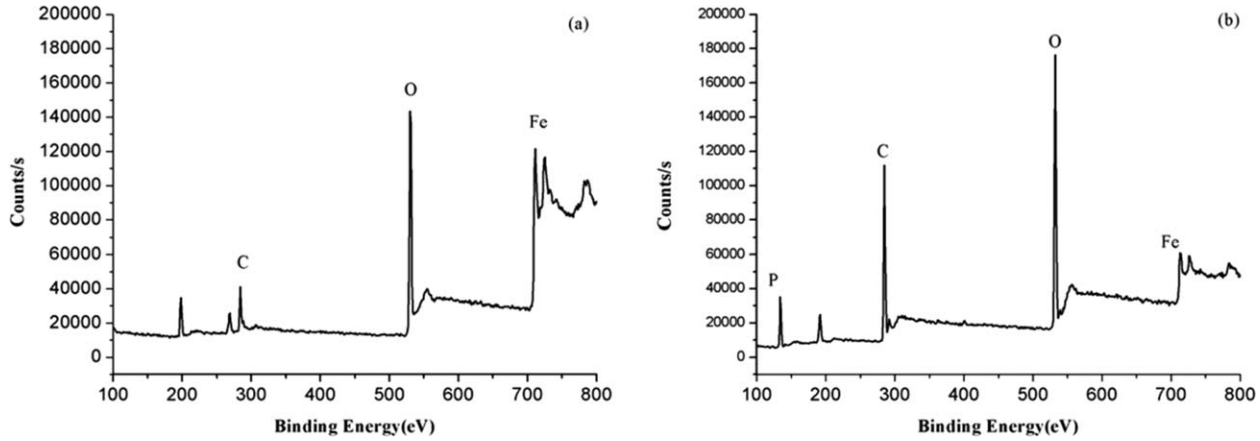

Figure 3. XPS of (a) β-Fe(O)OH and (b) β-Fe(O)OPDCP.

modification with PDCP. By comparing the electron binding energy of the iron element (Figure 4), we found that the 2p3/2 and 2p1/2 orbital electron binding energy of iron elements in the modified samples were 711.3 and 724.6 eV, respectively; these corresponded to the typical surface binding energy peaks of Fe^{3+}. As shown in Figure 4, the electron binding energy peak of iron in the modified sample shifted to a higher energy direction compared to the peak positions of the iron element in β-Fe(O)OH; this indicated that PDCP reacted with the surface hydroxyl groups of the β-Fe(O)OH rather than being simply adsorbed on the surface of the β-Fe(O)OH.

FTIR spectroscopy is an important technique for studying functional groups attached to the β-Fe(O)OH surface. Figure 5 is the FTIR spectra of unmodified β-Fe(O)OH and β-Fe(O)OPDCP. Sorbed water contributed to the H—O—H banding region at about 1630 cm^{-1} and the OH stretching region of H_2O at about 3400 cm^{-1}.[13] This was supported by the following TGA results. In the FTIR spectrum of unmodified β-Fe(O)OH, the energy translational mode of akaganeite due to Fe—O stretching was observed at 432 and 481 cm^{-1}. The bands at 848 and 688 cm^{-1} were the libation modes of the two O—H…Cl hydrogen bonds present.[13–15] In the spectrum of β-Fe(O)OPDCP, characteristic absorptions at 751 and 774 cm^{-1} were attributed to the $—C_6H_5$ group, those at 1593 and 1480 cm^{-1} were assigned to the aromatic ring C=C bonds, bands at 1232 and 1212 cm^{-1} were ascribed to P—O—Φ, bands at 1449 and 1390 cm^{-1} were assigned to O=P(OR), and absorptions at 1090 and 1015 cm^{-1} were due to the P—O—C group of PDCP.[16] The Fe-O stretching vibrations were responsible for the bands at about 440 cm^{-1}.[15]

TGA results under the nitrogen atmosphere gave further evidence regarding the content of organic parts grafted on β-Fe(O)OH because the organic and β-Fe(O)OH parts had distinct thermal stabilities. The results are shown in Figure 6. The change in the sample weight within the temperature range from 50°C to about 180°C may have been due to the emission of H_2O. The change from 180°C to about 520°C was possibly due to the decomposition of β-Fe(O)OH. The weight loss process ceased at 520°C, even though heating was continued to 700°C. As a result, the stable residue could reasonably be ascribed to α-Fe_2O_3.[17] The sample of β-Fe(O)OPDCP revealed that the weight loss of the sample was 49 wt %. Discounting the weight loss of the unmodified β-Fe(O)OH, the content of PDCP reacting with β-Fe(O)OH was 26 wt %.

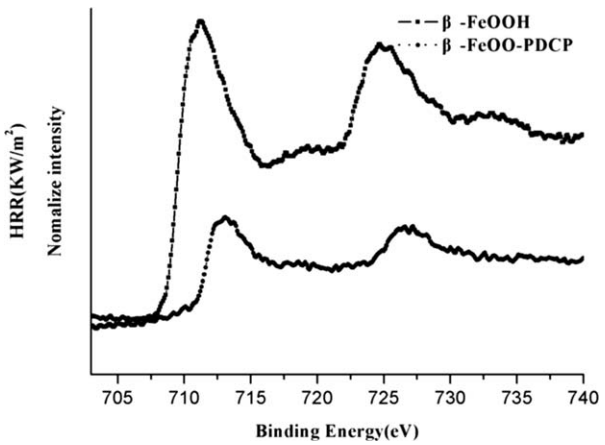

Figure 4. XPS spectra for the Fe region for the samples.

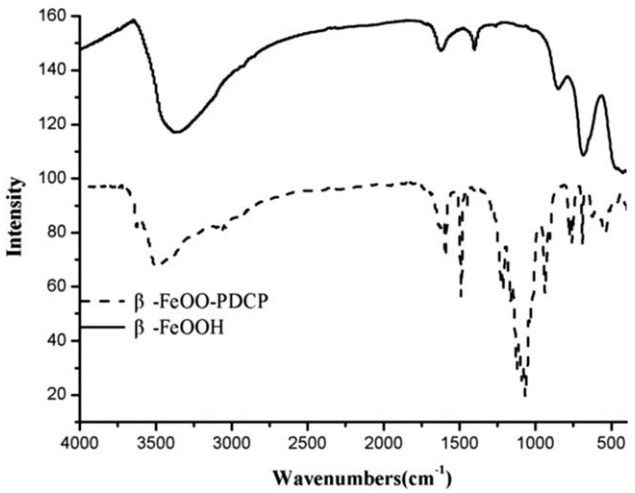

Figure 5. FTIR spectra of β-Fe(O)OH and β-Fe(O)OPDCP.

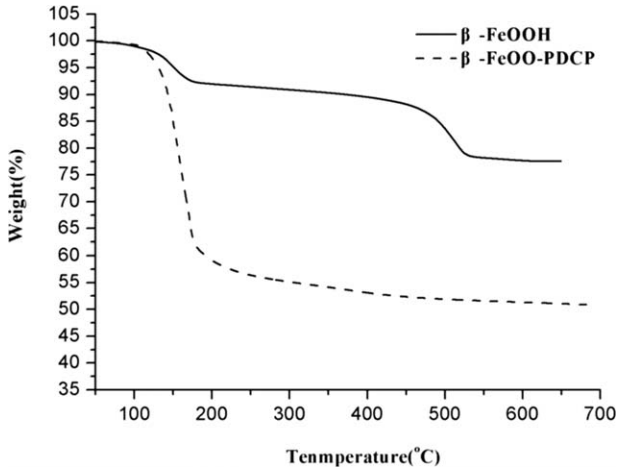

Figure 6. TGA curves of the β-Fe(O)OH and β-Fe(O)OPDCP samples.

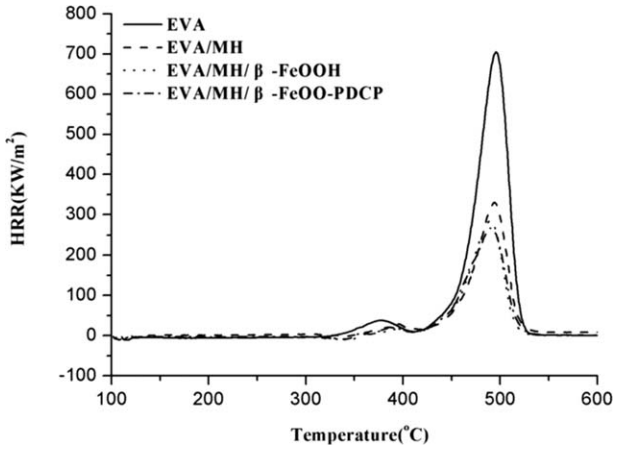

Figure 8. HRR curves of pure EVA, EVA/55% MH, EVA/54% MH/1% β-Fe(O) OH and EVA/54% MH/1% β-Fe(O)OPDCP samples.

Thermal Stability of the EVA, EVA/MH, and EVA/MH/Iron Compound Formulations

The thermal stability of synthesized samples was examined by thermogravimetry. The TGA and differential thermogravimetric (DTG) curves of the EVA and EVA composites under a nitrogen atmosphere are shown in Figure 7, and the data are summarized in Table I. The initial decomposition temperature was defined as the temperature at 10 wt % mass loss (T_{-10}), and we also recorded the temperature at 50 wt % mass loss (T_{-50}). It is was clear that the thermal degradation of the pure EVA and flame-retarded EVA composites were composed of two main steps. Compared with pure EVA, the flame-retarded EVA composites exhibited enhanced thermal behavior at temperatures ranging from 450 to 700°C and had large amounts of residues. The EVA3 and EVA4 systems both showed higher thermal stabilities and more yields of residue above 450°C. The reason for this could have been that the iron-containing composite acted as a Lewis acid, which could increase the intensity and compactness of the char layer, limit oxygen diffusion, and reduce the heat transfer through the char layer.[6] However, the Fe^{3+} ion also had same catalytic properties and increased the rate of EVA deacetylation.[18] So β-Fe(O)OH and β-Fe(O)OPDCP made the polymers more degradable at relatively low temperatures[19] and caused a higher thermal stability and more char residue above 450°C compared to those of the EVA2 composite.

Thermal Combustion Properties of the EVA, EVA/MH, and EVA/MH/Iron Compound Formulations

The thermal combustion properties of the EVA, EVA/MH, and EVA/MH/iron compound systems were characterized by MCC, which is an important method for obtaining intrinsic/material combustion properties. The HRR curves and heat-release data from MCC testing are shown in Figure 8 and Table II. EVA is a flammable polymeric composite, which has a high peak heat-release rate (PHRR), HRC, and total heat release (THR). A reduction in the PHRR of EVA2 was observed in the HRR curve (Figure 8 and Table II), which was caused by the effect of MH. When these two iron compounds were added to EVA/MH, the PHRR values all decreased. Compared with the value for EVA2, the values of EVA3 and EVA4 decreased to 14.0 and 19.5%, respectively.

HRC and THR are also important measures of the fire hazard of a material. From HRC and THR values for all systems

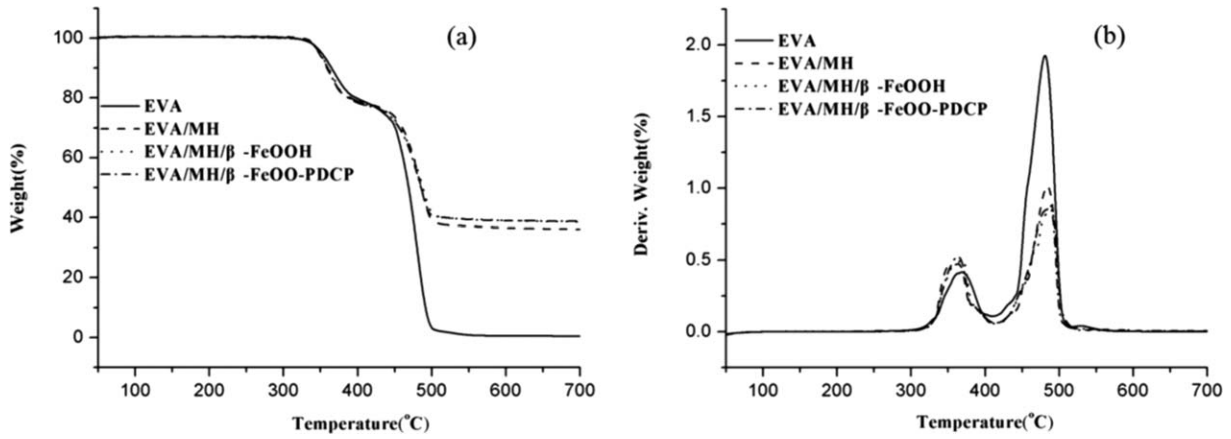

Figure 7. (a) TGA and (b) DTG curves of the pure EVA, EVA/55% MH, EVA/54% MH/1% β-Fe(O)OH, and EVA/54% MH/1% β-Fe(O)OPDCP samples.

Table II. MCC Data and the Results of UL-94 and LOI Testing of the EVA, EVA/MH, and EVA/MH/Iron Compound Formulations

	Calculated MCC data				UL-94, 3.2-mm bar		
Sample	HRC (J g^{-1}·k^{-1})	THR (kJ/g)	PHRR (W/g)	LOI	t_1/t_2[c](s)	Dripping	Rating
EVA1	713.0	30.7	706.0	17 ± 0.5	—[a]	Yes	NR[b]
EVA2	332.0	14.3	331.0	26 ± 0.5	15.0/5.5	Yes	NR[b]
EVA3	279.0	13.5	284.7	35 ± 0.5	14.5/3.5	No	V-2
EVA4	278.0	13.5	266.4	39 ± 0.5	8.5/1.4	No	V-0

[a] The specimen burned completely, and therefore, t_1 and t_2 were not detectable.
[b] NR, no rating.
[c] t_1 and t_2, average combustion times after the first and second applications of the flame.

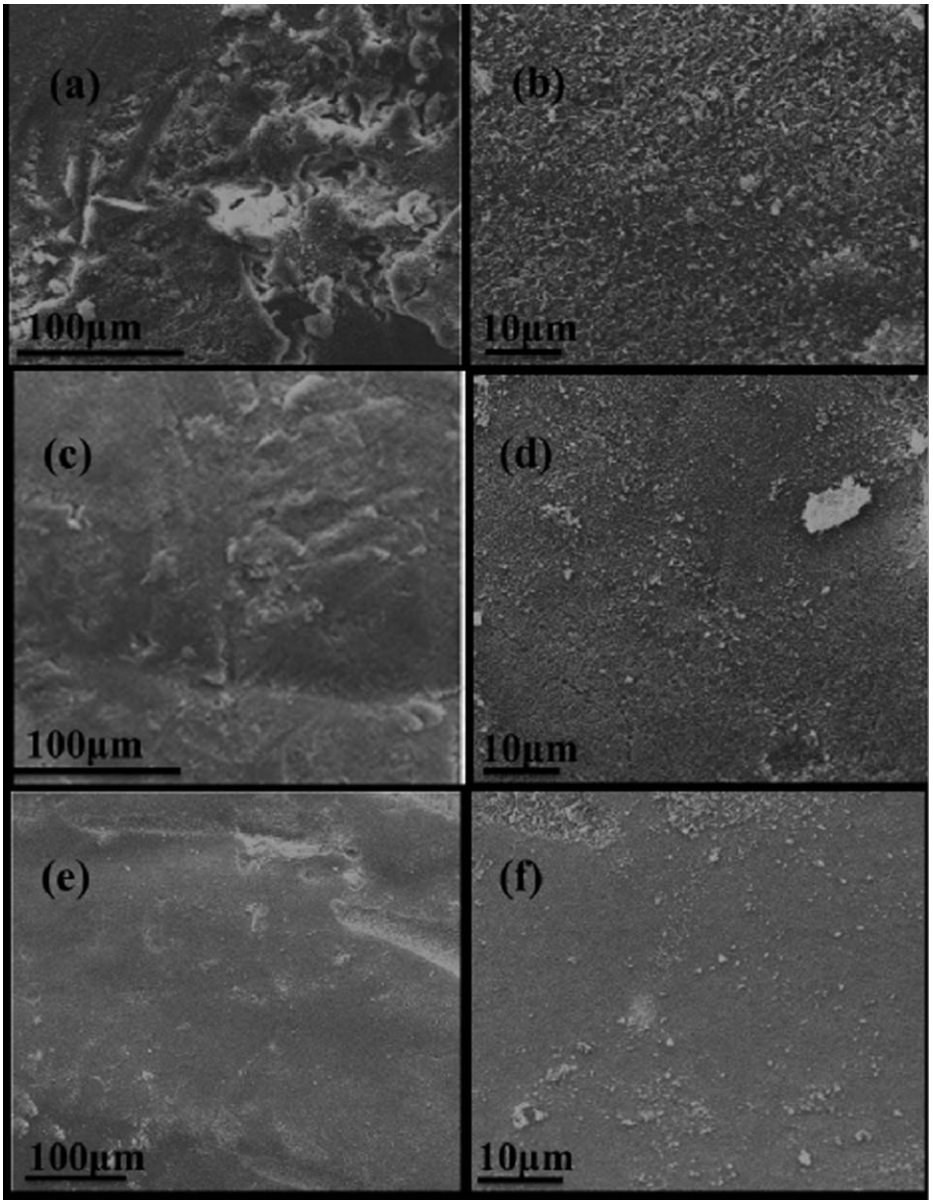

Figure 9. SEM of the char: ((a)(b))EVA/55% MH, ((c)(d))EVA/54% MH/1% β-Fe(O) OH and ((e)(f)) EVA/54% MH/1% β-Fe(O)OPDCP samples.

Table III. Comparison of the Dynamic Mechanical Thermal Properties and the Mechanical Properties of the EVA/MH, EVA/MH/β-Fe(O)OH, and EVA/MH/β-Fe(O)OPDCP Formulations

Sample	Tan δ (°C)	E′ (MPa) at the glass-transition region (e.g., at −4°C)	TS (MPa)	E_b (%)
EVA2	−4.2	1099.6	9.4	600.0
EVA3	1.2	1340.9	9.9	610.0
EVA4	−2.1	1823.8	10.8	750.0

(Table II), it was clearly observed that the largest reduction was still attributed to the composite in combination with MH. Compared with EVA1, the HRC and THR values of EVA2 were reduced by 53 and 53%, and those values for EVA4 decreased by 62 and 57%, respectively.

Fire Performances of the EVA, EVA/MH, and EVA/MH/Iron Compound Formulations

LOI and UL 94 tests were performed to determine the flame class of each system. The results are summarized in Table II. EVA is a flammable polymeric material with a lower LOI value. In the UL 94 test, EVA could not self-extinguish and showed serious dripping in the first application of the flame. Although the presence of 55% MH reduced flammability of the material according to the UL 94 test, the value of LOI indicated that the flammability of the MH-containing composite was clearly lower than that of the basic copolymer. The effects in that field were even better when the iron compounds were used. For example, EVA3 and EVA4 achieved V-2 and V-0 classifications, respectively, in the UL 94 test, and the LOI values for EVA3 and EVA4 increased to 35 and 39%, respectively. The results also show that as a certain fraction of β-Fe(O)OH was replaced by β-Fe(O)OPDCP, a significant increase in the LOI value and a better classification in the UL 94 test were obtained. This indicated that the fire risk of the EVA4 composite was the smallest.

Morphology of the Char Residue of the EVA/MH, EVA/MH/β-Fe(O)OH, and EVA/MH/β-Fe(O)OPDCP

Figure 9 shows the SEM micrographs of the char residue of EVA/MH and EVA/MH versus the loading of the β-Fe(O)OH or β-Fe(O)OPDCP systems. To elucidate the relationship between the microstructure of protective char and flame retardancy, three different kinds of char residues were collected from LOI tests. The microstructure of the char residue containing β-Fe(O)OPDCP [Figure 9(e,f)] displayed a more homogeneous and compact structure compared to that of the EVA3 system [Figure 9(c,d)], which had a small number of crevasses on the surface. There were many crevasses and holes on the surface of the char residue of the EVA2 composite [Figure 9(a,b)]; therefore, during burning, heat and flammable volatiles could easily penetrate the char layer into the flame zone. On the contrary, the char residue of the EVA4 system almost had no flaw, and the char layer seemed thicker and more solid than those of the other systems; this may effectively stop the transfer of heat and flammable volatiles and lead to a good flame retardancy.[20] A promising development in MH or something with the aid of iron-containing compounds, such as β-Fe(O)OPDCP, is expected anyway.

Mechanical Properties

The TS and E_b values of the EVA systems are shown in Table III. The TS and E_b values of the EVA4 system increased compared with those of the EVA3 system. The modified flame-retardant-filled EVA system had higher mechanical properties than the raw-flame-retardant-filled EVA composites. After modification by PDCP, the β-Fe(O)OPDCP may have enhanced the interfacial compatibility between the filler and EVA matrix and achieved a uniform dispersion of filler in the EVA matrix.[21] Therefore, the mechanical properties of the EVA4 system improved greatly.

Dynamic Mechanical Thermal Properties

The loss tangent (tan δ) and storage modulus (E′) values of the tested fire-retarded composites as a function of the temperature are presented in Figures 10 and 11, respectively. The data are summarized in Table III. The temperature at the maximum tan δ peak was considered to be the glass-transition temperature (T_g). Figure 10 reveals that the EVA3 system showed higher T_g values than the EVA/MH system; this was due to the rigid filler system, which limited the mobility of the polymer chains. The EVA4 system demonstrated relatively lower T_g values compared to that of the EVA3 system; this was because β-Fe(O)OH was modified by a flexible PDCP. As shown in Figure 11, the EVA3 system at the glass-transition region had a higher E′ than the EVA2 composite. It could be explained that β-Fe(O)OH was the rigid filler, which imparted stiffness behavior to the EVA/MH composite. However, E′ of the EVA4 system was higher than that of the EVA3 system in the glass-transition region. This may have been a result of the presence of PDCP, which enhanced the interfacial compatibility between the filler and the EVA matrix system.[21]

Volatilized Product Analysis

TGA–IR spectrometry was performed to analyze the volatilized products after the thermal decomposition of samples and

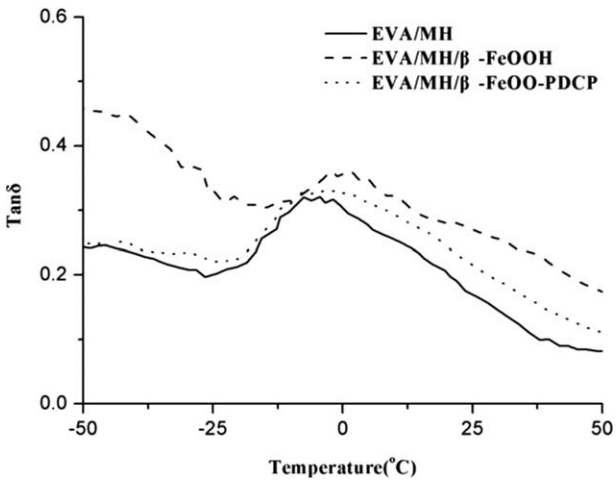

Figure 10. Tan δ versus temperature curves of EVA/55% MH, EVA/54% MH/1% β-Fe (O)OH and EVA/54% MH/1% β-Fe(O)OPDCP samples.

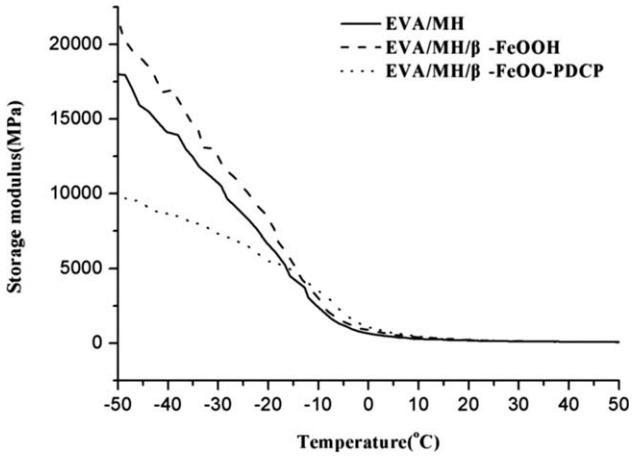

Figure 11. E' of EVA/55% MH, EVA/54% MH/1% β-Fe(O)OH and EVA/54% MH/1% β-Fe(O)OPDCP samples.

helped us to study the thermal degradation process. In this study, this method was used to make a comparison between the EVA2 and EVA4 systems. Some specific volatilized products were selected to study, including hydrocarbon (2985 cm^{-1}), acetate (1736 cm^{-1}), and CO (2180 cm^{-1}). The intensities of absorbance were all normalized to the samples' contents.

Figure 12 shows the change in the pyrolysis products at different times. For the total volatilized curves, we found that the intensity of the volatilized product dropped greatly with the presence of β-Fe(O)OPDCP. The hydrocarbon, acetate, and CO compounds shared a similar trend. The CO emission for the EVA4 composite decreased, indicating the reduction of toxic gases. What is more, the decrease in the hydrocarbon volatiles further led to the inhibition of smoke.[22] The reduced amount of volatiles could be explained by the fact that β-Fe(O)OPDCP had more effect in the condensed phase on char forming; this was useful for preventing the transfer of mass and heat.[6] Therefore, 1%β-Fe(O)OPDCP helped EVA/54% MH to improve the flame retardancy.

Combined with the previously analysis and the previous studies,[3,4] we concluded that on the one hand, the decomposition of MH could absorb the heat of the combustion surface when it was heated (340–490°). It could release large amounts of water to dilute the combustible surface oxygen; then, magnesium oxide was attached to the combustible surface to prevent further burning. On the other hand, the addition of β-Fe(O)OH or β-Fe(O)OPDCP enhanced the carbonization of the EVA/MH composite in the thermal decomposition process and reduced the mass loss rate. The condensed-phase products resulting from the carbonization reaction may have covered the residues

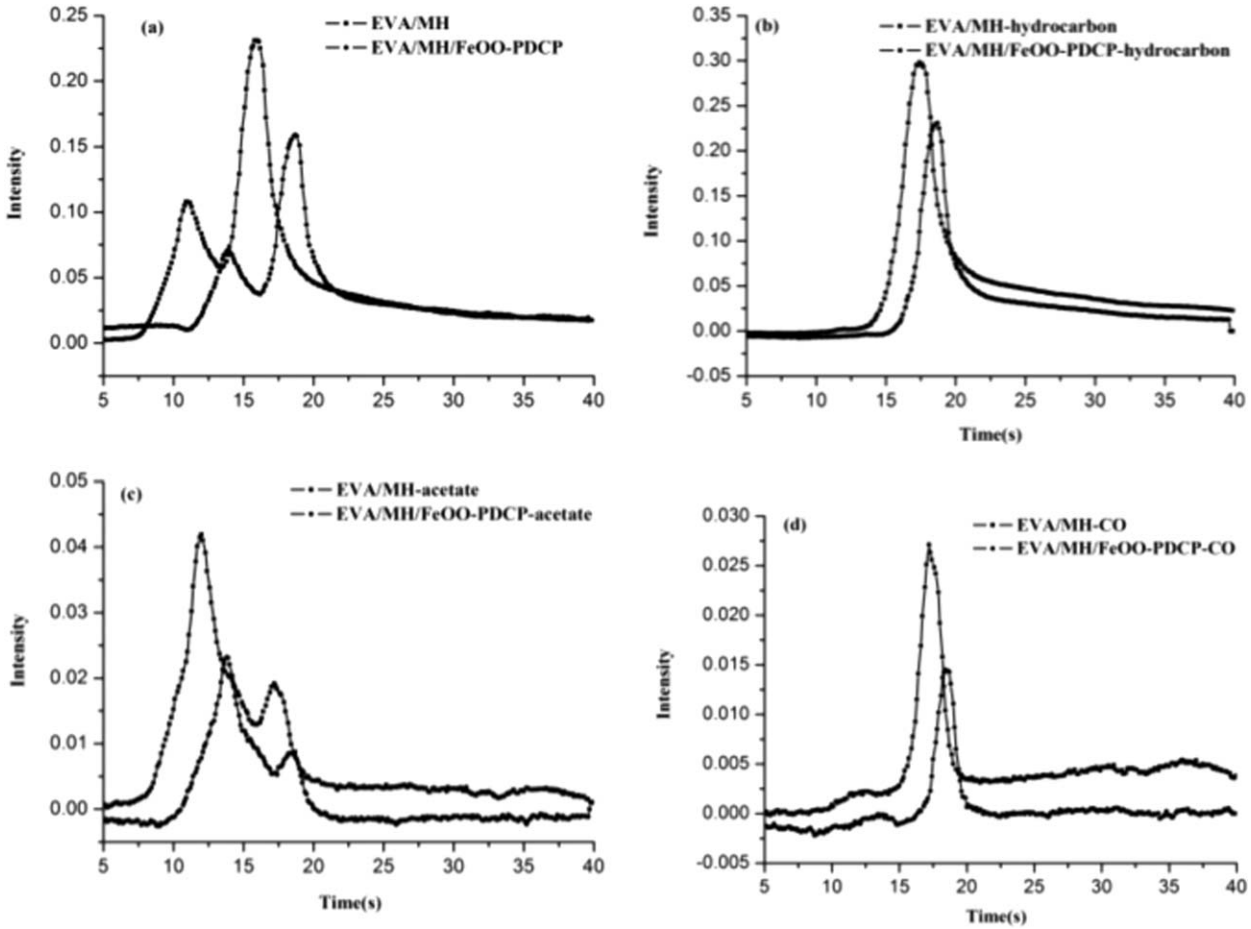

Figure 12. (a) Total (b) hydrocarbon (c) acetate (d) CO of EVA/55% MH and EVA/54% MH/1% β-Fe(O)OPDCP samples.

to obstruct or cut off the mass transfer path and reduce the concentration of combustible gases. Therefore, the fire hazards were further reduced by the introduction of β-Fe(O)OH or β-Fe(O)OPDCP.

CONCLUSIONS

In this study, the EVA/MH/β-Fe(O)OH or β-Fe(O)OPDCP systems were prepared through a melt-blending process. We found that the presence of β-Fe(O)OH and β-Fe(O)OPDCP both improved the char yields and thermal stability of the EVA/MH composite at higher temperatures. The MCC data showed that the PHRR, THR, and HRC values of the EVA3 and EVA4 systems were reduced compared to those of the EVA2 system. In comparison with the UL 94 V-2 rating of the EVA3 system, the EVA4 system passed the V-0 rating. Also, the EVA4 system obtained more significant improvements in LOI. The homogeneous and solid structure of char residue caused by β-Fe(O)OPDCP was observed by SEM. Furthermore, the EVA4 system demonstrated higher mechanical properties than the EVA3 system; this was due to the fact that β-Fe(O)OPDCP improved the interfacial compatibility between the fillers and EVA matrix. The results of TGA–IR show that β-Fe(O)OPDCP reduced the intensity of combustible volatilized products of the EVA/MH composite and left more carbon char. That means β-Fe(O)OPDCP may have been more capable of initiating a compact and homogeneous char on the surface, which turned out to be most important for the flame-retardant performance.

ACKNOWLEDGMENTS

This study was substantially supported by grants from National Basic Research Program of China (973 Program) (2012CB719701), Specialized Research Fund for the Doctoral Program of Higher Education (20103402110006) and the Research Grant Council of the Hong Kong Special Administrative Region, China (contract grant number CityU 122612).

REFERENCES

1. Holmes, M. *Plast. Addit. Compd.* **2004**, *6*, 32.
2. Sen, A. K.; Mukherjee, B.; Bhattacharya, A. S.; L. Sanghi, De, P. P.; Bhowmick, K. J. *Appl. Polym. Sci.* **1991**, *43*, 1673.
3. Montezin, F.; Lopez-Cuesta, J. M.; Crespy, A.; Georlette, P. *Fire Master* **1997**, *21*, 245.
4. Gheysari, D.; Behjat, A. *Eur. Polym. J.* **2002**, *38*, 1087.
5. Hassan, M. A. *Polym. Plast. Technol. Eng.* **2004**, *43*, 1487.
6. Zhang, Y.; Hu, Y.; Song, L.; Wu, J.; Fang S. L. *Polym. Adv. Technol.* **2008**, *19*, 960.
7. Nie, S. B.; Song, L.; Zhan, J.; Hu, Y.; Tai, Q. L.; Chen, L. J. *J. Macromol. Sci. A* **2011**, *46*, 554.
8. Wang, L.; Yang, W.; Wang, B. B.; Wu, Y.; Hu, Y.; Song, L.; Yuen, R. K. K. *Ind. Eng. Chem. Res.* **2012**, *51*, 7884.
9. Lu, H. D.; Song, L.; Hu, Y. *Polym. Adv. Technol.* **2011**, *22*, 379.
10. Guo, P. Z.; Tan, J. S.; Ji, Q. Q.; Zhao, D.; Zhao, X. S. *Chin. J. Inorg. Chem.* **2009**, *4*, 647.
11. Riveros, P. A.; Dutrizac, J. E. *Hydrometallurgy* **1997**, 1–2, 85.
12. Music, S.; Krehula, S.; Popovic, S. *Mater. Lett.* **2004**, *58*, 444.
13. Deliyanni, E. A.; Bakoyannakis, D. N.; Zouboulis, A. I.; Matis, K. A.; Nalbandian, L. *Micropor. Mesopor. Mater.* **2001**, *42*, 49.
14. Yusan, S.; Erenturk, S. A. *Desalination* **2010**, *263*, 233.
15. Deliyanni, E. A.; Nalbandian, L.; Matis, K. A. *J. Colloid Interface Sci.* **2006**, *302*, 458.
16. Liu, Y.; Zhang, Y.; Cao, Z. H.; Fang, Z. P. *Ind. Eng. Chem. Res.* **2012**, *51*, 11059.
17. Wang, X.; Chen, X. Y.; Gao, L. S.; Zheng, H. G.; Ji, M. R.; Tang, C. M.; Shen, T.; Zhang, Z. D. *J. Mater. Chem.* **2004**, *14*, 905.
18. Zhu, J.; Uhl, F. M.; Morgan, A. B.; Wilkie, C. A. *Chem. Mater.* **2001**, *13*, 4649.
19. Pranav, N.; Priya, D.; Matt, L.; Mikhail, Y. G. R.; Benjamin, S. H.; Miriam, R.; Anatoly, F.; Andy, H. T.; Jeffrey, W. G.; Syed, K. *Polymer* **2007**, *48*, 827.
20. Wang, D. Y.; Cai, X. X.; Qu, M. H.; Liu, Y.; Wang, J. S.; Wang, Y. Z. *Polym. Degrad. Stab.* **2008**, *93*, 2186.
21. Wang, B. B.; Hu, S.; Zhao, K. M.; Lu, H. D.; Song, L.; Hu, Y. *Ind. Eng. Chem. Res.* **2011**, *50*, 11476.
22. Dong, Y. Y.; Gui, Z.; Hu, Y.; Wu, Y.; Jiang, S. H. *J. Hazard Mater.* **2012**, *34*, 209.